Title

Evaluation of Young's Modulus of Tethered 1–Palmitoyl-2-oleoyl-sn-glycero-3-phosphocholine Membranes Using Atomic Force Spectroscopy

Journal

The Journal of Physical Chemistry C, 118(50)

ISSN

1932-7447

Authors

Wang, Xi

Sanderson, Robert N

Ragan, Regina

Publication Date

2014-12-18

DOI

10.1021/jp505451h

THE JOURNAL OF PHYSICAL CHEMISTRY C

Article

pubs.acs.org/JPCC

Evaluation of Young's Modulus of Tethered 1-Palmitoyl-2-oleoyl-*sn*-glycero-3-phosphocholine Membranes Using Atomic Force Spectroscopy

Xi Wang,[†,§] Robert N. Sanderson,[‡,§] and Regina Ragan*[,†]

[†]Department of Chemical Engineering and Materials Science and [‡]Department of Physics and Astronomy, University of California—Irvine, Irvine, California 92697-2575, United States

ABSTRACT: Unilamellar vesicles composed of 1-palmitoyl-2-oleoyl-*sn*-glycero-3-phosphocholine (POPC) with varying 1,2-distearoyl-*sn*-glycero-3-phosphoethanolamine-*N*-poly(ethylene glycol)-2000-*N*-[3-(2-pyridyldithio) propionate] (DSPE-PEG-PDP) concentration between 0 mol % and 24 mol % were assembled on atomically flat template-stripped gold (TS Au) surfaces. Force spectroscopy, using an atomic force microscope (AFM), of the resulting tethered lipid bilayer membranes (tLBMs) in buffer provided information regarding mechanical response as a function of tethering molecule, DSPE-PEG-PDP, concentration. Young's modulus was determined by fitting the force−indentation curve with a recently modified Sneddon model that corrects for contributions from the substrate underneath. At low concentrations, Young's modulus is lower than that of a supported POPC LBM, i.e., directly sitting on a solid substrate. The decrease in modulus is attributed to increased membrane fluidity as coupling between the tLBM and solid substrate is reduced by the incorporation of DSPE-PEG-PDP tethering groups. From the determined Young's modulus values, the PEG chain conformation is found to dominate tLBM rigidity at concentrations above 6 mol %. Analysis of AFM force spectroscopy data indicates that the poly(ethylene glycol) (PEG) mushroom to brush transition occurs near 6 mol %, and this leads to first softening and then abrupt stiffening of tLBMs at higher DSPE-PEG-PDP concentration associated with the transition. When DSPE-PEG-PDP concentration is increased to 24 mol %, AFM topography and Young's modulus appear correlated with another phase transition; AFM topography images are consistent with a bilayer disk structure with DSPE-PEG-PDP segregated at the rim of the disk.

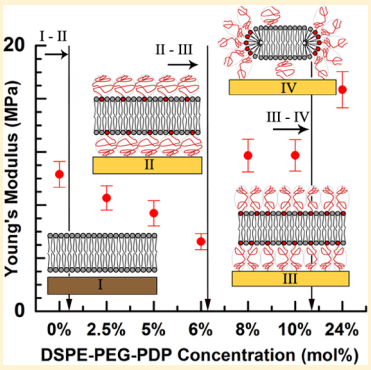

INTRODUCTION

Lipid bilayer membranes (LBMs) are a system of considerable research interest since early work showing their formation on solid supports[1] and the ability to probe systems electrically[2] and to study molecular events during membrane−membrane interactions.[3] Incorporation of a polymer cushion layer between LBMs and substrates has been shown to alleviate both immobility of transmembrane proteins and reduced lipid diffusion rates that are observed in solid supported LBMs[4] providing a platform for studying biological processes in controlled systems.[5−8] The tethered lipid bilayer membrane (tLBM) is one type of hybrid bilayer membrane whose chemical affinity between the LBM and the solid substrate stabilizes the system and can provide a hydrated spacer layer between the LBM and substrate. Poly(ethylene glycol) (PEG) has been commonly used as a polymer cushion layer as it produces fluidic and stable LBMs.[9−11] LBMs have become an important tool to understand biological mechanisms such as a function of photosynthetic membrane proteins,[12] intercellular signaling,[13] and small-molecule interactions with membrane surfaces[14] and to create single virus sensors.[15]

Here we investigate the mechanical properties of the tLBM on gold (Au) electrodes assembled using vesicle fusion. tLBMs are formed by incorporating 1,2-distearoyl-*sn*-glycero-3-phosphoethanolamine-*N*-poly(ethylene glycol)-2000-*N*-[3-(2-pyridyldithio) propionate] (DSPE-PEG-PDP) molecules into 1-palmitoyl-2-oleoyl-*sn*-glycero-3-phosphocholine (POPC) vesicles to affect vesicle substrate interactions in order to facilitate vesicle fusion.[11,16] The concentration of DSPE-PEG-PDP tethering molecules is varied, and we investigate the resulting changes in morphology and mechanical properties using atomic force spectroscopy and analysis of force−separation data with analytical models. Understanding the mechanical properties of LBMs is important as this parameter plays a role in several membrane-mediated biological processes. Molecular dynamics simulations have shown that lateral pressure in membranes affects protein function,[17−19] and protein binding produces an asymmetrical mechanical response in the membrane.[20] Nonspecific interactions with surrounding lipids and proteins such as membrane curvature and elastic moduli affect the function of ATP-binding cassette (ABC) proteins,[21] mechanosensitive ion channels important in bacterial membrane defense against lysis,[22] and mechanotransduction was found to initiate ATP release in urothelial

Special Issue: John C. Hemminger Festschrift

Received: June 3, 2014
Revised: September 3, 2014
Published: September 5, 2014

dx.doi.org/10.1021/jp505451h | J. Phys. Chem. C 2014, 118, 29301−29309

cells.[23] Variations of Young's modulus have been found between malignant cancer cells and normal cells.[24−26]

Atomic force microscopy (AFM), since shortly after its invention, has been an important tool to image cells with nanometer resolution under physiological conditions[27] with pico-Newton force sensitivity,[28,29] and combined with fluorescence microscopy nanoscale, imaging of cellular receptors is possible.[30] The nanoindentation function, where the AFM tip compresses the sample and records the resulting force as a function of indentation, allows for measuring local elastic properties of membranes and vesicles.[24−26,31−33] Uncertainties in the tip−sample contact point, assumptions in theoretical models, and instrument uncertainties can affect the accuracy of determined moduli from force spectroscopy data.[34] Recently Wagner et al. found that the calibration of the sensitivity of the photodiode dominated instrument uncertainty rather than uncertainties in the cantilever stiffness or Z-piezo calibration.[35] However, this can be minimized by calibrating on a clean surface,[36] and thus we address the latter two issues here.

The mechanical properties of untethered POPC LBM on mica and tLBM of POPC with varying DSPE-PEG-PDP concentration from 2.5 to 24 mol % on Au were studied and compared using AFM force spectroscopy. Previously we found that higher DSPE-PEG-PDP concentration in large unilamellar vesicles (LUVs) facilitated vesicle fusion on TS Au surfaces.[16] It was found that DSPE-PEG-PDP concentrations in LUV required less force for tLBM formation, and this was attributed to an increase in LUV−substrate interactions, and mechanical properties were not studied. Here we compare the Sneddon[37] (semi-infinite sample contacted by a paraboloidal-shaped tip) with a new modified model, Bottom Effect Cone Correction,[38] that corrects for the thickness-dependent influence of the interaction of a sharp AFM tip with a hard substrate on measured mechanical response[39] of LBMs. We also provide new algorithms for determining the tip−sample contact point, as misidentification of the contact point can lead to errors in determined mechanical properties.[34,40] Young's modulus (E) of tLBMs was determined by fitting experimental data to Sneddon and Bottom Effect Cone Correction (BECC) models. E was found to be directly correlated with PEG chain conformation. Results show an initial decrease in tLBM elastic modulus with respect to supported POPC LBM then an abrupt increase at DSPE-PEG-PDP concentration of 8% after the mushroom to brush transition has been reported to occur.[41,42] Incorporating higher concentrations of DSPE-PEG-PDP, up to 24%, results in a further increase in E, and a structural change, also associated with a phase transition, is observed in AFM topography. AFM topography data indicate that PEG chains segregate at the rim of bilayer disks at 24% DSPE-PEG-PDP concentration. Analysis of force spectroscopy data with the BECC model provides a cleaner signature of the phase transition points than the Sneddon model. These studies provide a systematic method to probe local mechanical properties and phase transitions of thin film polymers, biological membranes, and cellular structure using sharp AFM tips while mitigating influence from the hard substrate underneath and errors in determining the contact point.

MATERIALS AND METHODS

Materials. 1-Palmitoyl-2-oleoyl-*sn*-glycero-3-phosphocholine (POPC) and 1,2-distearoyl-*sn*-glycero-3-phosphoethanolamine-*N*-poly(ethylene glycol)-2000-*N*-[3-(2-pyridyldithio) propionate] (DSPE-PEG-PDP) were obtained from Avanti Polar Lipids (Alabaster, AL). HEPES at >99.5% purity and chloroform at >99.8% purity were purchased from Sigma-Aldrich (St. Louis, MO). NaCl at >99.0% purity was from Fisher Scientific Inc. (Pittsburgh, PA). Water used in this study was purified with a Milli-Q water system (≥18.2 MΩ.cm, Millipore Corp., Billerica, MA). All chemicals were used as received.

Preparation of Unilamellar Vesicles. Large unilamellar vesicles were prepared following an extrusion method.[8,43] Vesicles composed primarily of POPC lipids with (i) 0% (ii) 2.5% (iii) 5% (iv) 6% (v) 8% (vi) 10% and (vii) 24% DSPE-PEG-PDP were prepared. DSPE-PEG-PDP and POPC lipids were dissolved at specified molar ratios in chloroform at 1 mg/mL for stock solutions. Lipid−chloroform mixtures were dried on the bottom of a glass vial by a gentle stream of nitrogen and desiccated in vacuum for at least 1 h to completely remove chloroform. Then, the dried lipid mixtures were rehydrated by the addition of HEPES buffer (5 mM HEPES, pH 7.4, with 150 mM NaCl) to yield a final lipid concentration of 5 mM. The resulting lipid suspensions were then subjected to five freeze−thaw cycles and extruded 15 times through two polycarbonate membranes with a pore size of 100 nm using a syringe-type extruder (Avanti Polar Lipids, Alabaster, AL).

Sample Preparation. A tethered LBM refers to a membrane that is linked to a substrate via chemical bonding, while an untethered LBM indicates no chemical bond formation between the LBM and substrate. Untethered LBMs, or simply LBMs, were prepared by depositing a 100 μL aliquot of vesicle suspension composed of 0% DSPE-PEG-PDP/100% POPC on mica. Mica was freshly cleaved with scotch tape immediately prior to use. TLBMs with varied DSPE-PEG-PDP concentration were prepared at room temperature by depositing a 100 μL aliquot of vesicle suspension with lipid composition of (i) 2.5% DSPE-PEG-PDP/97.5% POPC, (ii) 5% DSPE-PEG-PDP/95% POPC, (iii) 6% DSPE-PEG-PDP/94% POPC, (iv) 8% DSPE-PEG-PDP/92% POPC, (v) 10% DSPE-PEG-PDP/90% POPC, and (vi) 24% DSPE-PEG-PDP/76% POPC on an 8 mm × 8 mm Au substrate. Au substrates were prepared using the facile method of the template stripping method to create a pristine and atomically flat surface for membrane assembly.[11,44] All samples were incubated at room temperature for 30 min. After incubation, samples were rinsed with 200 μL of HEPES buffer 4 times and glued to a glass slide for AFM characterization. Sample surfaces remained hydrated in HEPES buffer at all times during sample preparation and AFM characterization.

Atomic Force Microscopy Imaging and Force Spectroscopy. Both AFM imaging and force spectroscopy were performed using a MFP-3D-Bio AFM (Asylum Research, Santa Barbara, CA) in an acoustic isolation enclosure. Commercial silicon nitride AFM probes (OMCL-TR 400 PSA, Olympus) with pyramid-shaped tips and Au coating on the reflective side of the cantilever were used for all AFM measurements. The tip radius of curvature is 20 ± 5 nm as provided by the manufacturer. Both AFM imaging and force spectroscopy were carried out at a temperature of 23 ± 1 °C in HEPES buffer. AFM images were acquired under tapping mode with a scan speed of 1.0 Hz. All topography images were rendered with background slopes corrected using Igor Pro software v 6.0.

AFM force spectroscopy was performed in contact mode. The nominal spring constant of the AFM cantilever specified by manufacturer is 0.08 N/m. Before acquiring force measurement data, the AFM cantilever spring constant was calibrated by

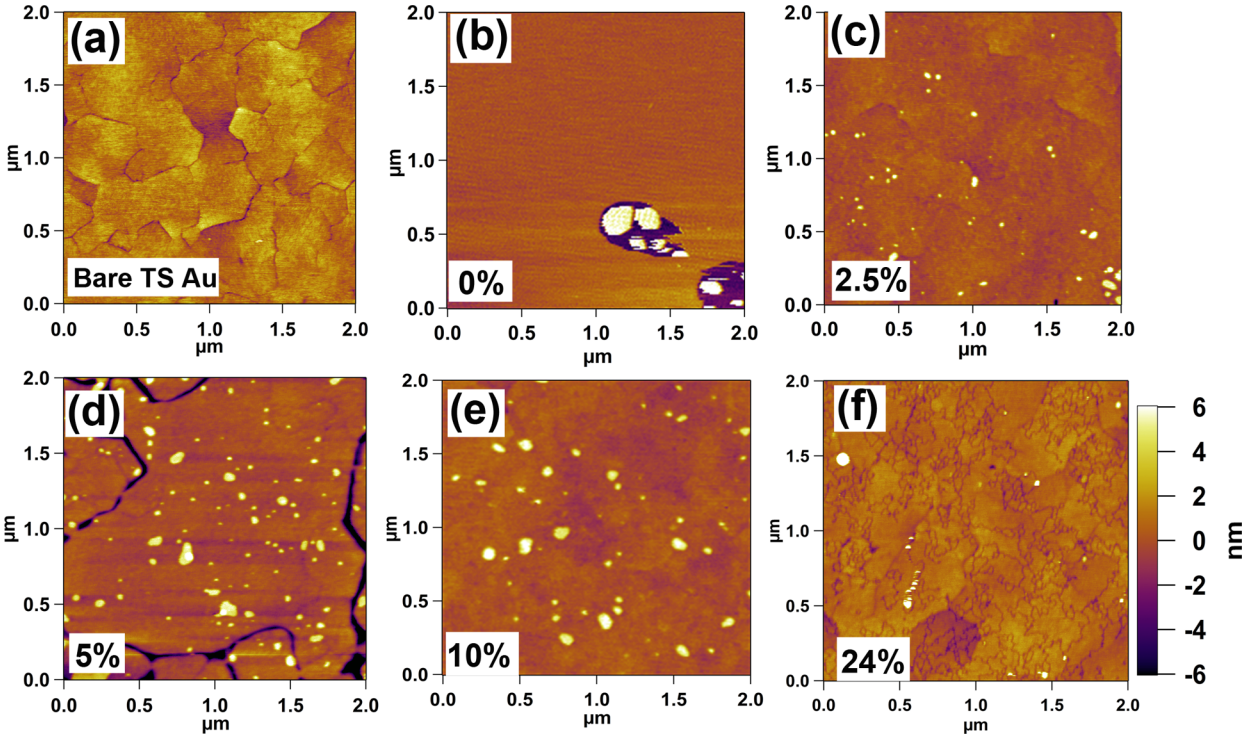

Figure 1. Tapping mode AFM topography images of (a) bare TS Au; (b) mica after incubation with vesicles composed of 100% POPC; and TS Au after incubation with vesicles composed of (c) 2.5% DSPE-PEG-PDP/97.5% POPC, (d) 5% DSPE-PEG-PDP/95% POPC, (e) 10% DSPE-PEG-PDP/90% POPC, and (f) 24% DSPE-PEG-PDP/76% POPC.

measuring deflection against a freshly stripped TS Au substrate to minimize surface contaminants and then calculated by the thermal noise method.[45] Force measurements were obtained on randomly chosen positions on tLBM covered substrates. Force measurements were performed with an approaching speed of 1.8 μm/s.

Analysis of Force–Separation Data. Force–separation data obtained from AFM force spectroscopy were analyzed using an algorithm developed within the framework of Wolfram Mathematica 9.0. The algorithm was designed to import force vs separation data and to output LBM and tLBM thickness and Young's modulus using the two models, Sneddon and Bottom Effect Cone Correction (BECC). Identification of the AFM tip/LBM contact point was achieved by determining the change in force–separation behavior from a polynomial (predicted by the above two models) to an exponential decay that is related to long-range electrostatic interactions and interactions with the polymer brush. The contact point was iterated until the theoretically expected fit to the experimental curves was within one standard deviation. Data points near this contact point were then fitted to Sneddon and BECC models of tip–LBM interaction using least-squares methods to find the elastic modulus of the tLBM.

RESULTS AND DISCUSSION

Formation of LBMs as a Function of DSPE-PEG-PDP Concentration. Large unilamellar vesicles of POPC with DSPE-PEG-PDP concentration ranging from 0% to 24% were prepared in HEPES buffer. In the case of pure POPC vesicles, these were deposited on mica since POPC vesicles do not spontaneously fuse to form LBM on plasma-treated TS Au but simply adsorb.[11] POPC vesicles with varied DSPE-PEG-PDP tethering molecule concentration, ranging from 2.5% to 24%, were incubated on TS Au surfaces as described above and in our previous work.[11] It was found that tLBMs form on TS Au via Au–thiolate interactions between the disulfide bond in the PDP group and the Au substrate; the process can be assisted with an external force of an AFM probe.[16] In this prior work higher DSPE-PEG-PDP concentrations in vesicles required less force for tLBM formation that was attributed to increased vesicle substrate interactions, and mechanical properties were not evaluated. Here we examine how the morphology and mechanical properties are affected by increasing the concentration of the tethering molecule. Figure 1 shows 2 μm × 2 μm AFM topography images of (a) TS Au, (b) POPC LBM on on mica, and (c–f) tLBM on TS Au with varying DSPE-PEG-PDP concentration.

Subtle changes in topography can be observed in the AFM images of Figure 1. In Figure 1a, the surface topography of a typical TS Au substrate is shown having low root-mean-square roughness, less than 0.6 nm over 2 μm × 2 μm. An AFM topography image of mica after 30 min incubation of POPC vesicles and rinsing with HEPES buffer is shown in Figure 1b. This image exhibits flat featureless regions corresponding to a POPC LBM and a few bright regions, indicating unruptured vesicles incorporated in the LBM. Figure 1c–f shows AFM topography images of TS Au after 30 min incubation with POPC vesicles containing 2.5%, 5%, 10%, and 24% DSPE-PEG-PDP, respectively. AFM images after vesicle fusion with vesicles having DSPE-PEG-PDP concentration from 2.5% to 10% are consistent with large area tLBM formation. Yet when further increasing DSPE-PEG-PDP concentration to 24% in POPC vesicles, domain boundaries are observed in the AFM image of Figure 1f. These domains vary in size from approximately 50 nm up to 400 nm in diameter, and the domain boundaries exhibit high, local curvature and are

dx.doi.org/10.1021/jp505451h | J. Phys. Chem. C 2014, 118, 29301–29309

different from the domain boundaries of bare TS Au (shown in Figure 1a) and thus are not attributable to the TS Au surface morphology. For reference, Figure 1d provides an example of how Au defects interrupt tLBMs when the TS Au surface preparation is not optimized, and one can observe that the features differ from those in Figure 1f. (Note that Au domains can be increased by annealing such that large defect-free areas can be obtained.[46,47])

AFM force spectroscopy measurements were also performed on samples shown in Figure 1 to gain insight into the origin of different observed surface morphology. Representative force−separation curves obtained from tLBMs with DSPE-PEG-PDP concentration varying from 0% to 24% are shown in Figure 2.

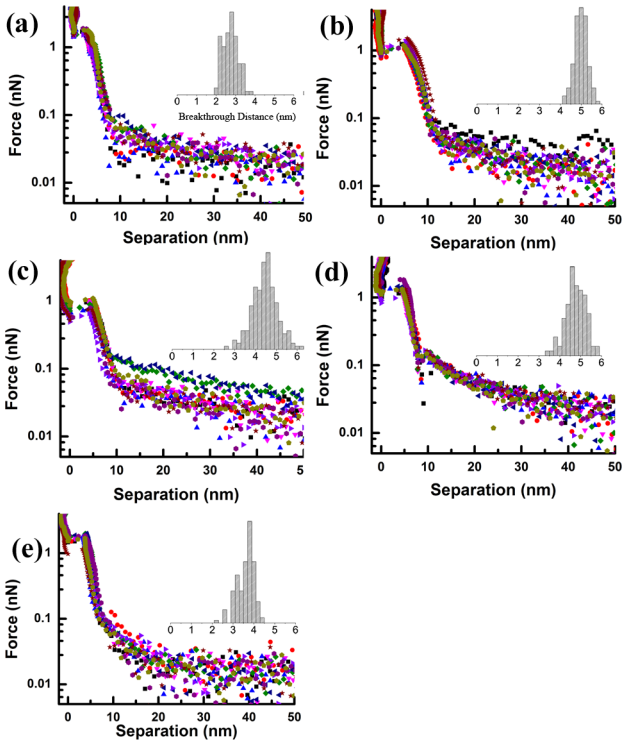

Figure 2. Representative force−separation curves in semilog scale obtained from (a) 100% POPC LBM on mica and tLBM with (b) 2.5% DPSE-PEG-PDP/97.5% POPC, (c) 8% DSPE-PEG-PDP/92% POPC, (d) 10% DSPE-PEG-PDP/90% POPC, and (e) 24% DSPE-PEG-PDP/76% POPC. Each force−separation plot in b−f includes ten curves from each sample. The insets are histograms of the breakthrough distance (in nm) determined from force−separation curves.

The AFM tip interaction with a hard wall (TS Au surface) is used as the reference point.[48] All the curves show the characteristic breakthrough events attributed to an AFM tip penetrating a membrane on a hard surface.[33] The breakthrough distance measures the thickness of a compressed LBM under the force applied by the AFM tip.[49] Average measured distances from breakthrough events from force−separation data are listed in Table 1. Histograms of measured breakthrough distances from $n \geq 150$ curves are shown as insets in Figure 2. The average breakthrough distance of the LBM composed of pure POPC is 2.9 ± 0.4 nm (n = 150) in agreement with values previously observed.[11] From these curves, the average breakthrough distance for DSPE-PEG-PDP concentration between 2.5% and 10% was determined to be approximately the same, approximately 4.5 nm as observed previously.[11,41] At DSPE-PEG-PDP concentration of 24%, the breakthrough distance decreases to 3.5 ± 0.5 nm.

It is well-known that the breakthrough distance underestimates the total thickness of LBM.[48,50] For example, the thickness for the pure POPC membrane is calculated to be 3.9 nm,[51,52] whereas the compressed LBM thickness measured via a breakthrough event is 2.9 nm. The total LBM thickness with hydration and spacer layer can be determined from the force−separation curve between the onset compression point and the hard wall contact point.[41,48] To obtain a statistically representative view of the samples, more than 150 force curves were analyzed for each data set in this study, necessitating the use of computational algorithms for data analysis. For each force curve, tLBM thickness was calculated using an iterative method. The batches of force−separation curves were analyzed using an algorithm implemented with Wolfram Mathematica 9.0. The hardwall (point A) and breakthrough (point B) locations were located by looking for the slope changes associated with the characteristic large jump in tip−sample separation as illustrated in Figure 3a between points "A" and "B". The contact point (point C) was found by first performing a quadratic fit, as per the Sneddon Model,[37] representing the force on the AFM tip, on the data points to the right of point B (see Figure 3b). This is the first estimate of the location of the contact point that underestimates the LBM/tLBM thickness. The points immediately to the right of this first iteration of the contact point were then fitted to an exponential decay representing the longer-range interaction, such as electrostatic forces[33] and interaction with the polymer brush,[53] between the AFM tip and the LBM surface. The contact point was then iterated if the data to the right of the contact point deviated from an exponential fit by more than a standard deviation. The iteration continued until the fit beyond the contact point was within one standard deviation of an exponential fit. This provides a more accurate method to examine relative thicknesses of tLBMs as a function of DSPE-PEG-PDP concentration which is important to determine accurate values of elastic moduli.

As listed in Table 1, the total LBM thickness estimated for 100% POPC LBM determined from the onset compression point to the hard wall contact point is 8.8 ± 1.1 nm, which is consistent with small-angle neutron scattering measurements[54] for determination of POPC thickness and considering that an approximate 2 nm water layer is present between the hydrophilic substrate and the inner leaflet of the LBM.[55,56]

Table 1. List of tLBM Breakthrough Distances and Onset Compression Distances Using the Hard Wall Substrate Contact for Reference As Measured from AFM Force−Separation As a Function of DSPE-PEG-PDP Concentration[a]

	0%	2.5%	5%	6%	8%	10%	24%
breakthrough distance (nm)	2.9 ± 0.4	5.0 ± 0.3	4.6 ± 0.5	4.1 ± 0.7	4.4 ± 0.8	4.8 ± 0.6	3.5 ± 0.5
onset compression distance (nm)	8.8 ± 1.1	11.0 ± 0.6	9.2 ± 0.9	9.6 ± 1.4	10.0 ± 1.2	9.4 ± 1.03	8.2 ± 1.0

[a]Each listed value is the average mean determined from 150 different force−separation curves with the standard deviation also listed.

dx.doi.org/10.1021/jp505451h | J. Phys. Chem. C 2014, 118, 29301−29309

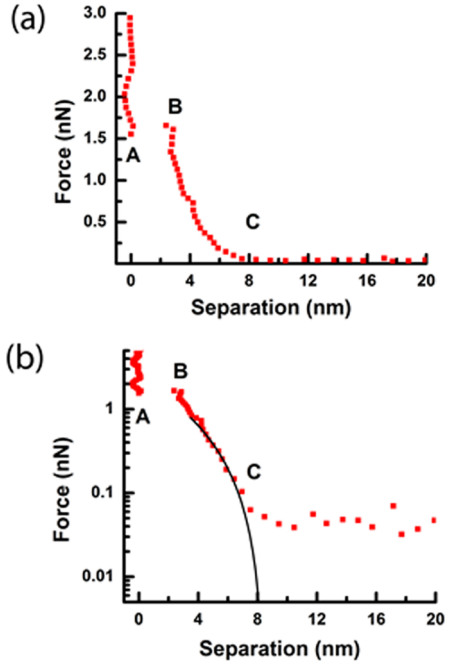

Figure 3. (a) Characteristic force–separation curve. (b) Semilog force–separation curve with an overlay of a quadratic fit used to find the contact point.

The force–separation curves for tLBMs with DSPE-PEG-PDP concentration ranging from 2.5% to 8% are not clearly distinguishable considering uncertainty in the thickness estimation. The estimated thickness is approximately 10 nm indicating an additional 2 nm hydration layer due to the tethering molecules. A slight decrease in thickness is observed at 10% (the estimated thickness of tLBMs formed from 10% DSPE-PEG-PDP/90% POPC vesicles is 9.4 ± 1.0 nm), and then a large decrease to 8.2 ± 1.0 nm for tLBMs formed from 24% DSPE-PEG-PDP/76% POPC vesicles. The latter has an estimated thickness significantly smaller than those of lower DSPE-PEG-PDP concentrations and overlaps that of pure POPC. This abrupt thickness decrease indicates a structure change in the membrane at vesicle composition between 10% and 24% DSPE-PEG-PDP concentration.

AFM Tip–PEG Polymer Interaction. In order to further understand tLBM structure evolution with DSPE-PEG-PDP concentration, force–separation curves collected from tLBMs with varied concentrations were plotted in log-scale to expand the initial tip–sample interaction region. Note that in Figure 2a–e ten data sets are plotted in each image to show the trends are reproducible. Backmann et al. studied conformational changes in PEG layers using AFM force spectroscopy; they observed an exponentially decaying long-range repulsive force when PEG was in the brush phase and a shorter range repulsive force when PEG was in the mushroom phase.[57] For example, in Figure 2a, pure POPC LBMs on mica show an abrupt slope after the onset of the repulsive force as there are no PEG groups on the surface. At low DSPE-PEG-PDP concentration (2.5%), the force–separation curve shown in Figure 2b does not differ significantly from pure POPC, indicating PEG polymer chains on the tLBM surface are in the mushroom phase. At higher DSPE-PEG-PDP concentration (8% and 10%), the long-range repulsive force increases in magnitude as observed in Figure 2c and 2d, thus indicating the AFM tip is interacting with a PEG polymer brush on tLBMs, though this is not a clear signature of a transition. A reverse trend occurs at DSPE-PEG-PDP concentration of 24%, and the overlaid force–separation curves in Figure 2e have an exponential tail lower in magnitude similar to pure POPC (Figure 2a). These data suggest that PEG polymer brushes are of lower density at DSPE-PEG-PDP concentration of 24% than 8% or 10%. This interaction was consistently observed in force–separation

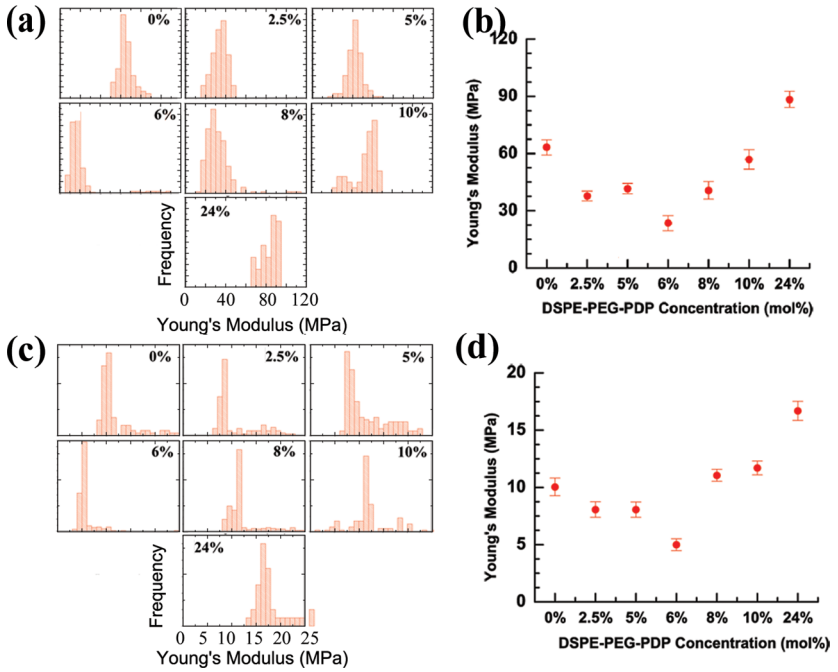

Figure 4. Histograms of the determined values of Young's modulus by fitting force–separation curves using the (a) Sneddon and (c) BECC models. Plot of tLBM Young's moduli as a function of DSPE-PEG-PDP concentration determined from force spectroscopy data by fitting the (b) Sneddon and (d) BECC model. The error bars represent the deviation in the measurements and fits.

dx.doi.org/10.1021/jp505451h | J. Phys. Chem. C 2014, 118, 29301–29309

curves of tLBMs with 24% DSPE-PEG-PDP as observed in the overlaid data of Figure 2e; in addition all the curves at this highest measured concentration showed onset compression distance values similar to pure POPC on mica. Considering the observed changes in AFM topography in Figure 1f, changes in breakthrough distance, and total estimated thickness, a change in structure of tLBMS with 24% DSPE-PEG-PDP occurs that has not been observed before for tLBMs.

Determination of the Young's Moduli of tLBMs with Different DSPE-PEG-PDP Concentration. In order to further understand differences in AFM data for tLBMs as a function of DSPE-PEG-PDP concentration, Young's modulus (E) of tLBM was extracted by first fitting force−indentation curves with the Sneddon model that assumes a conical shaped tip.[37] The relationship of the load (F_{cone}) versus indentation depth (δ) using the Sneddon model is given by

$$F_{cone} = \frac{2}{\pi} \tan \alpha \frac{E}{1 - \upsilon^2} \delta^2 \quad (1)$$

where α is the opening angle of a conical tip (35° in this study); E is the Young's modulus of the film; and ν is the Poisson's ratio of tLBMs equal to 0.5 assuming a perfectly incompressible material in response to uniaxial strain.[34,39] With the contact point identified, the exponential long-range interaction was subtracted from the force data, and the data were then fit to the Sneddon model. Figure 4a shows histograms of the values of Young's modulus as determined from the Sneddon model. Figure 4b is the plot of E as a function of DSPE-PEG-PDP concentration determined by fitting force spectroscopy data to the Sneddon model. Each E value plotted in Figure 4b is an average from those calculated from the slope of at least 150 force−indentation curves. For comparison, force spectroscopy data were also fit to a model, using the same method described above that is a modification of the Sneddon model called the "bottom effect cone correction" (BECC) that accounts for contribution of the substrate stiffness that leads to overestimation of E when fitting data acquired with a sharp AFM tip for polymer thin films or cell membranes.[38]

$$F_{BECC} = \frac{8}{3\pi} E \tan \theta \delta^2 \left(1 + 1.7795 \frac{2 \tan \theta}{\pi^2} \frac{\delta}{h} + 16(1.7795)^2 \tan^2 \theta \frac{\delta^2}{h^2} \right) \quad (2)$$

Histograms of the value of Young's modulus determined from the BECC model and the resulting average value with standard deviation are shown in Figure 4c and 4d, respectively. Qualitatively, in Figure 4b and 4d, one can observe that fitting of the data with both models shows an initial decrease in E with the addition of DSPE-PEG-PDP and then an increase at the highest concentrations. It is also immediately evident that E values are higher when analyzed with the Sneddon model[37] versus BECC model.[38] It is expected as the BECC model utilizes the Betti−Rayleigh reciprocal theorem to correct for finite thickness differences that influence analysis of force spectroscopy data and lead to higher values of E. The influence of the hard substrate on E values is expected to be greater as the thickness of films/membranes decreases.[38,39] Notice that the pure POPC data (onset compression distance of 8.8 nm) have a greater overestimation of the mean value of E, 63 ± 4.0 MPa from the Sneddon model and 10.0 ± 0.8 MPa from the BECC model, than 2.5% DSPE-PEG-PDP (onset compression distance of 11.0 nm), 38 ± 2.5 MPa from the Sneddon model and 8.1 ± 0.7 MPa from the BECC model. The decrease of E with the incorporation of DSPE-PEG-PDP is reflective of a PEG polymer cushion separating LBMs from TS Au substrates and is an indirect indication of increased membrane fluidity for tLBMs with respect to solid supported LBMs. Comparing the E values for tLBMs of Figure 4 to published results, Picas et al. reported E values of dioleoyl PC/dipalmitoyl PC (DOPC/DPPC) LBM on mica with an E value of 19.3 and 28.1 MPa for liquid and gel phases, respectively.[58]

Further increases of DSPE-PEG-PDP concentration up to 6% show a further decrease of E to 5.0 ± 0.5 MPa. (Note that from this point on mean values of E from only the BECC model will be referred to in the text.) The reduction in membrane rigidity at 6% DSPE-PEG-PDP concentration that is evident in both models suggests that a PEG mushroom to brush transition occurs near this concentration due to an increase in disorder in tLBMs at the phase transition. This is further substantiated by the abrupt increase in E at 8% DSPE-PEG-PDP, 11.0 ± 0.5 MPa, which overlaps with that for tLBMs containing 10% DSPE-PEG-PDP, 11.7 ± 0.6 MPa. The observed increase in E is consistent with incorporated PEG chains in the brush conformation as the brush conformation is less compressible than in the mushroom conformation.[41] The transition from the mushroom to brush above 6% DSPE-PEG-PDP concentration is consistent with prior results. DSPE-PEG in hydro soy PC (HSPC) vesicles was found to undergo the mushroom to brush transition at a concentration of 6 mol %.[42] Fluorescence recovery after photobleaching results of 8% DOPE-PEG LBM showed no recovery.[41] It is well-known that PEG polymers undergo a mushroom-to-brush transition when the surface density increases beyond the Flory radius. The Flory radius of the polymer is given by[59]

$$R_F = a \cdot N^{3/5} \quad (3)$$

where a is the length of a subunit and N is the number of subunits. The DSPE-PEG-PDP molecule used in this study has 45 PEG subunits with length of approximately 3.5 Å.[60] Thus, R_F is calculated as 3.4 nm for PEG in DSPE-PEG-PDP. In order to estimate the surface density as a function of DSPE-PEG-PDP concentration in tLBMs, de Gennes theory[61] is used where the average distance between grafting sites (D) is governed by

$$D = \left(\frac{A}{f} \right)^{1/2} \quad (4)$$

A is the mean molecular area, and f is the mole fraction of DSPE-PEG-PDP lipids in the tLBM. The mean molecular area for a POPC lipid is approximately in the range of 50−70 Å^2.[60] When D is greater than R_F, PEG chains are predicted to be in a random coil conformation (mushroom phase) with PEG chain length (L) equal to R_F (3.4 nm), while when D is less than R_F, PEG groups are predicted to be in an extended conformation (brush phase) due to lateral repulsion.[62] From eq 3, the PEG mushroom to brush transition would be expected to occur at DSPE-PEG-PDP concentration of 4.3−6.1%. Therefore, at the DSPE-PEG-PDP concentration less than or equal to approximately 6%, one would expect the PEG chain to be in the mushroom regime. The AFM force spectroscopy data clearly reflect this transition and narrow down the composition where it occurs as there is an abrupt increase in E above 6% concentration. The consistent increased E values of tLBMs at 8% and 10% DSPE-PEG-PDP concentration indicate that the

dx.doi.org/10.1021/jp505451h | J. Phys. Chem. C 2014, 118, 29301−29309

PEG polymer chain conformation can dominate tLBM stiffness. Note that the values listed for the onset compression distance do not include the polymer brush on the surface of tLBMs as the characteristic interaction between an AFM tip and polymer brush is in the exponential term of the repulsive interaction.[53] Thus, we would only expect small changes in onset compression distance values with the mushroom to brush transition that are within experimental and fitting error. We do see a very slight increase in the breakthrough distance at 10% DSPE-PEG-PDP (4.8 ± 0.6 nm) than lower concentrations such as 8% (4.4 ± 0.8 nm) as the more closely packed PEG groups may become constrained and exhibit a different interaction with the AFM tip. Analysis of dense PEG brushes on Au surfaces found an increase in stiffness within 5 nm of the surface and a deviation from the exponential decay of the repulsive force predicted in de Gennes theory to quadratic behavior in this regime.[53] This would explain why the onset compression distances do not vary significantly. The semilog plots of force−separation in Figure 2c and 2d, for 8% and 10% DSPE-PEG-PDP concentration, clearly show an increase in the magnitude of the long-range repulsive force as a signature of PEG groups in the brush phase.[57]

At DSPE-PEG-PDP concentration of 24%, E further increases to 16.7 ± 0.8 MPa indicating another phase transition. This observed stiffening at 24% DSPE-PEG-PDP concentration is consistent with a structural transition. The AFM topography and force spectroscopy data where a change in the morphology and breakthrough distance, respectively, of this membrane as compared to other membranes with differing DSPE-PEG-PDP concentrations is observed are also consistent with a structural transition. Edwards et al., using transmission electron microscopy (TEM), observed the structural transition of PEG-grated vesicles from a lamellar (liposome) structure to a disk-like structure, so-called bilayer disk, above 10 mol % PEG.[63] This transition from vesicles to micelles has been also observed in vesicles composed of DSPE/PEG[64] and DSPC/PEG (2000)[65] at PEG concentrations of 15−20% in solution. Johnsson et al. using cryogenic TEM measured a transition from vesicles to a discoidal micelle structure dominating near 20% PEG−lipid concentration.[66] The authors determined by correlating TEM and dynamic light scattering data with a "mixed-disk" model[67] that PEG appears to segregate to the edges to stabilize the edges.[66,67] The irregular boundaries of POPC membranes with 24% DSPE-PEG-PDP concentration observed in the AFM topography data of Figure 1f are consistent with segregation of PEG chains to the boundary of membrane domains. Thus, bilayer disk structures containing 24% DSPE-PEG-PDP molecules appear to attach on TS Au via the Au−thiolate bonding. Consistent with prior models of discoidal micelles[66,67] and the AFM images of Figure 1 and measured breakthrough distances for 24% DSPE-PEG-PDP, PEG chains appear to segregate to the disk rims; the total estimated membrane thickness with such a structure would be 7.3 nm which is consistent with the onset compression thickness determined using AFM force spectroscopy.

Figure 5 is a schematic illustration of structures of (a) untethered and (b−c) tethered LBM with varied DSPE-PEG-PDP concentrations based on the above analysis. Figure 5a illustrates a POPC LBM sitting on a mica substrate with a thin water layer in between. The proposed structure of tLBMs with DSPE-PEG-PDP concentration between 2.5% and 6% is shown in Figure 5b where DSPE-PEG-PDP, with PEG chains in the mushroom phase, is present on both sides of the tLBM. The

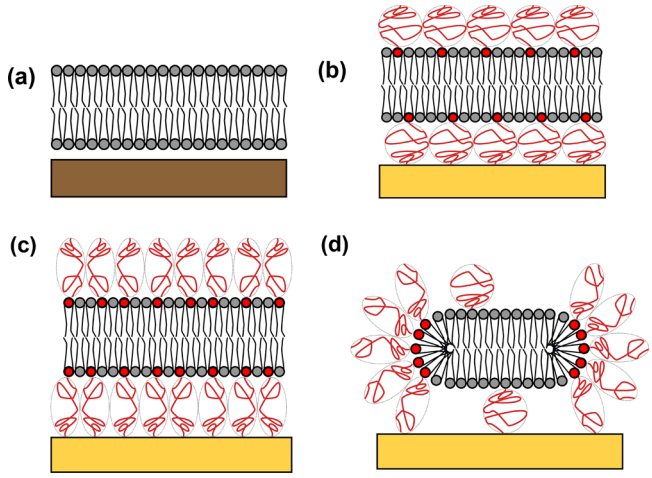

Figure 5. Schematic illustration of tLBM structures with lipid composition of (a) 100% POPC; (b) 1−6% DSPE-PEG-PDP/99−95% POPC; (c) 8−10% DSPE-PEG-PDP/92−90% POPC, and (d) 24% DSPE-PEG-PDP/76% POPC.

structure of tLBM composed of 8% DSPE-PEG-PDP/92% POPC and 10% DSPE-PEG-PDP/90% POPC (Figure 5c) has a similar structure as shown in Figure 5b, with the only difference being that PEG chains are in the brush conformation. When the DSPE-PEG-PDP concentration was increased to 24%, Figure 5d illustrates bilayer disks that attach to the TS Au substrate from solution where the DSPE-PEG-PDP molecules segregate to the rim of the disk. The proposed tLBM structures are in good agreement with the topography, relative onset compression thicknesses, and the fitted Young's modulus.

CONCLUSION

In this study, Young's moduli (E) of tLBMs as a function of DSPE-PEG-PDP tethering molecule concentration are determined using AFM topography and analysis of AFM force spectroscopy data. Incorporating a polymer cushion layer, PEG, between POPC LBM and the solid substrate significantly decreases tLBM stiffness compared to the solid supported POPC LBM. The lowest tLBM stiffness appears to be correlated with disorder near the PEG mushroom to brush phase transition at 6 mol %. There is an abrupt increase in E after the mushroom to brush phase transition occurs due to increased PEG grafting density. At 24% DSPE-PEG-PDP, the tLBM structure appears to change to a flattened micelle disk on the Au substrates, and this phase transition is also reflected in an increase in E. The variation of E, determined from fitting the Sneddon model and the BECC model, follows the same qualitative trend. However, the BECC model yields lower values for E, alleviating the contribution of the hard substrate underneath the tLBM, and reflects the variation of E with the phase transitions more clearly. In addition to providing a systematic method to study local mechanical properties of biological membranes with sharp AFM tips, this study also provides a tLBM platform with controllable membrane rigidity, which could be used as a cell model to study mechanosensitive protein/peptide−membrane interactions as a function of membrane mechanical properties. This study demonstrates that AFM force spectroscopy alongside appropriate analysis can be used to determine mechanical properties of biological membranes. Methods to determine local mechanical properties

dx.doi.org/10.1021/jp505451h | J. Phys. Chem. C 2014, 118, 29301−29309

will aid future studies such as understanding how this parameter affects regulation of transmembrane proteins.

AUTHOR INFORMATION

Corresponding Author

*Telephone: (949) 824-6830. Fax: (949) 824-2541. E-mail: rragan@uci.edu.

Author Contributions

§These authors contributed equally to this work.

Notes

The authors declare no competing financial interest.

ACKNOWLEDGMENTS

We thank Asylum Research Technical Support (Asylum Research, Santa Barbara, CA) for valuable discussions regarding AFM force spectroscopy principles. We acknowledge James Dolas and Hang Fu from the Department of Chemical Engineering and Materials Science, UC Irvine, for assistance with data rendering and compilation. This work was supported by the National Science Foundation (CHE-0748912).

REFERENCES

(1) Brian, A. A.; McConnell, H. M. Allogeneic Stimulation of Cytotoxic T Cells by Supported Planar Membranes. *Proc. Natl. Acad. Sci. U.S.A.* **1984**, *81*, 6159−6163.

(2) Stelzle, M.; Sackmann, E. Sensitive Detection of Protein Adsorption to Supported Lipid Bilayers by Frequency-Dependent Capacitance Measurements and Microelectrophoresis. *Biochim. Biophys. Acta, Biomembr.* **1989**, *981*, 135−142.

(3) McConnell, H. M.; Watts, T. H.; Weis, R. M.; Brian, A. A. Supported Planar Membranes in Studies of Cell-Cell Recognition in the Immune System. *Biochim. Biophys. Acta, Rev. Biomembr.* **1986**, *864*, 95−106.

(4) Dietrich, C.; Tampé, R. Charge Determination of Membrane Molecules in Polymer-Supported Lipid Layers. *Biochim. Biophys. Acta, Biomembr.* **1995**, *1238*, 183−191.

(5) Cornell, B. A.; Braach-Maksvytis, V. L. B.; King, L. G.; Osman, P. D. J.; Raguse, B.; Wieczorek, L.; Pace, R. J. A Biosensor That Uses Ion-Channel Switches. *Nature* **1997**, *387*, 580−583.

(6) Naumann, C. A.; Prucker, O.; Lehmann, T.; Rühe, J.; Knoll, W.; Frank, C. W. The Polymer-Supported Phospholipid Bilayer: Tethering as a New Approach to Substrate−Membrane Stabilization. *Biomacromolecules* **2002**, *3*, 27−35.

(7) Kühner, M.; Tampé, R.; Sackmann, E. Lipid Mono- and Bilayer Supported on Polymer Films: Composite Polymer-Lipid Films on Solid Substrates. *Biophys. J.* **1994**, *67*, 217−226.

(8) Wagner, M. L.; Tamm, L. K. Tethered Polymer-Supported Planar Lipid Bilayers for Reconstitution of Integral Membrane Proteins: Silane-Polyethyleneglycol-Lipid as a Cushion and Covalent Linker. *Biophys. J.* **2000**, *79*, 1400−1414.

(9) Albertorio, F.; Diaz, A. J.; Yang, T.; Chapa, V. A.; Kataoka, S.; Castellana, E. T.; Cremer, P. S. Fluid and Air-Stable Lipopolymer Membranes for Biosensor Applications. *Langmuir* **2005**, *21*, 7476−7482.

(10) Munro, J. C.; Frank, C. W. In Situ Formation and Characterization of Poly(ethylene Glycol)-Supported Lipid Bilayers on Gold Surfaces. *Langmuir* **2004**, *20*, 10567−10575.

(11) Wang, X.; Shindel, M. M.; Wang, S.-W.; Ragan, R. A Facile Approach for Assembling Lipid Bilayer Membranes on Template-Stripped Gold. *Langmuir* **2010**, *26*, 18239−18245.

(12) Sumino, A.; Dewa, T.; Takeuchi, T.; Sugiura, R.; Sasaki, N.; Misawa, N.; Tero, R.; Urisu, T.; Gardiner, A. T.; Cogdell, R. J.; et al. Construction and Structural Analysis of Tethered Lipid Bilayer Containing Photosynthetic Antenna Proteins for Functional Analysis. *Biomacromolecules* **2011**, *12*, 2850−2858.

(13) Nair, P. M.; Salaita, K.; Petit, R. S.; Groves, J. T. Using Patterned Supported Lipid Membranes to Investigate the Role of Receptor Organization in Intercellular Signaling. *Nat. Protoc.* **2011**, *6*, 523−539.

(14) Huang, D.; Zhao, T.; Xu, W.; Yang, T.; Cremer, P. S. Sensing Small Molecule Interactions with Lipid Membranes by Local pH Modulation. *Anal. Chem.* **2013**, *85*, 10240−10248.

(15) Bally, M.; Graule, M.; Parra, F.; Larson, G.; Höök, F. A Virus Biosensor with Single Virus-Particle Sensitivity Based on Fluorescent Vesicle Labels and Equilibrium Fluctuation Analysis. *Biointerphases* **2013**, *8*, 4.

(16) Wang, X.; Shindel, M. M.; Wang, S.-W.; Ragan, R. Elucidating Driving Forces for Liposome Rupture: External Perturbations and Chemical Affinity. *Langmuir* **2012**, *28*, 7417−7427.

(17) Marsh, D. Lateral Pressure Profile, Spontaneous Curvature Frustration, and the Incorporation and Conformation of Proteins in Membranes. *Biophys. J.* **2007**, *93*, 3884−3899.

(18) Samuli Ollila, O. H.; Róg, T.; Karttunen, M.; Vattulainen, I. Role of Sterol Type on Lateral Pressure Profiles of Lipid Membranes Affecting Membrane Protein Functionality: Comparison between Cholesterol, Desmosterol, 7-Dehydrocholesterol and Ketosterol. *J. Struct. Biol.* **2007**, *159*, 311−323.

(19) Brown, M. F. Curvature Forces in Membrane Lipid-Protein Interactions. *Biochemistry (Moscow)* **2012**, *51*, 9782−9795.

(20) Maftouni, N.; Amininasab, M.; Ejtehadi, M. R.; Kowsari, F.; Dastvan, R. Nanomechanical Properties of Lipid Bilayer: Asymmetric Modulation of Lateral Pressure and Surface Tension due to Protein Insertion in One Leaflet of a Bilayer. *J. Chem. Phys.* **2013**, *138*, 065101.

(21) Clay, A. T.; Sharom, F. J. Lipid Bilayer Properties Control Membrane Partitioning, Binding, and Transport of P-Glycoprotein Substrates. *Biochemistry (Mosow.)* **2013**, *52*, 343−354.

(22) Nomura, T.; Cranfield, C. G.; Deplazes, E.; Owen, D. M.; Macmillan, A.; Battle, A. R.; Constantine, M.; Sokabe, M.; Martinac, B. Differential Effects of Lipids and Lyso-Lipids on the Mechanosensitivity of the Mechanosensitive Channels MscL and MscS. *Proc. Natl. Acad. Sci. U. S. A.* **2012**, *109*, 8770−8775.

(23) Olsen, S. M.; Stover, J. D.; Nagatomi, J. Examining the Role of Mechanosensitive Ion Channels in Pressure Mechanotransduction in Rat Bladder Urothelial Cells. *Ann. Biomed. Eng.* **2011**, *39*, 688−697.

(24) Lekka, M.; Laidler, P.; Gil, D.; Lekki, J.; Stachura, Z.; Hrynkiewicz, A. Z. Elasticity of Normal and Cancerous Human Bladder Cells Studied by Scanning Force Microscopy. *Eur. Biophys. J.* **1999**, *28*, 312−316.

(25) Lekka, M.; Pogoda, K.; Gostek, J.; Klymenko, O.; Prauzner-Bechcicki, S.; Wiltowska-Zuber, J.; Jaczewska, J.; Lekki, J.; Stachura, Z. Cancer Cell Recognition − Mechanical Phenotype. *Micron* **2012**, *43*, 1259−1266.

(26) Prabhune, M.; Belge, G.; Dotzauer, A.; Bullerdiek, J.; Radmacher, M. Comparison of Mechanical Properties of Normal and Malignant Thyroid Cells. *Micron* **2012**, *43*, 1267−1272.

(27) Butt, H.-J.; Wolff, E. K.; Gould, S. A. C.; Dixon Northern, B.; Peterson, C. M.; Hansma, P. K. Imaging Cells with the Atomic Force Microscope. *J. Struct. Biol.* **1990**, *105*, 54−61.

(28) Florin, E. L.; Moy, V. T.; Gaub, H. E. Adhesion Forces between Individual Ligand-Receptor Pairs. *Science* **1994**, *264*, 415−417.

(29) Te Riet, J.; Katan, A. J.; Rankl, C.; Stahl, S. W.; van Buul, A. M.; Phang, I. Y.; Gomez-Casado, A.; Schön, P.; Gerritsen, J. W.; Cambi, A.; et al. Interlaboratory Round Robin on Cantilever Calibration for AFM Force Spectroscopy. *Ultramicroscopy* **2011**, *111*, 1659−1669.

(30) Duman, M.; Pfleger, M.; Zhu, R.; Rankl, C.; Chtcheglova, L. A.; Neundlinger, I.; Bozna, B. L.; Mayer, B.; Salio, M.; Shepherd, D.; et al. Improved Localization of Cellular Membrane Receptors Using Combined Fluorescence Microscopy and Simultaneous Topography and Recognition Imaging. *Nanotechnology* **2010**, *21*, 115504.

(31) Li, S.; Eghiaian, F.; Sieben, C.; Herrmann, A.; Schaap, I. A. T. Bending and Puncturing the Influenza Lipid Envelope. *Biophys. J.* **2011**, *100*, 637−645.

(32) Calò, A.; Reguera, D.; Oncins, G.; Persuy, M.-A.; Sanz, G.; Lobasso, S.; Corcelli, A.; Pajot-Augy, E.; Gomila, G. Force Measure-

ments on Natural Membrane Nanovesicles Reveal a Composition-Independent, High Young's Modulus. *Nanoscale* **2014**, *6*, 2275−2285.
(33) Alessandrini, A.; Facci, P. Nanoscale Mechanical Properties of Lipid Bilayers and Their Relevance in Biomembrane Organization and Function. *Micron* **2012**, *43*, 1212−1223.
(34) Dimitriadis, E. K.; Horkay, F.; Maresca, J.; Kachar, B.; Chadwick, R. S. Determination of Elastic Moduli of Thin Layers of Soft Material Using the Atomic Force Microscope. *Biophys. J.* **2002**, *82*, 2798−2810.
(35) Wagner, R.; Moon, R.; Pratt, J.; Shaw, G.; Raman, A. Uncertainty Quantification in Nanomechanical Measurements Using the Atomic Force Microscope. *Nanotechnology* **2011**, *22*, 455703.
(36) McConney, M. E.; Singamaneni, S.; Tsukruk, V. V. Probing Soft Matter with the Atomic Force Microscopies: Imaging and Force Spectroscopy. *Polym. Rev.* **2010**, *50*, 235−286.
(37) Sneddon, I. N. The Relation between Load and Penetration in the Axisymmetric Boussinesq Problem for a Punch of Arbitrary Profile. *Int. J. Eng. Sci.* **1965**, *3*, 47−57.
(38) Gavara, N.; Chadwick, R. S. Determination of the Elastic Moduli of Thin Samples and Adherent Cells Using Conical Atomic Force Microscope Tips. *Nat. Nanotechnol.* **2012**, *7*, 733−736.
(39) Ngwa, W.; Chen, K.; Sahgal, A.; Stepanov, E. V.; Luo, W. Nanoscale Mechanics of Solid-Supported Multilayered Lipid Films by Force Measurement. *Thin Solid Films* **2008**, *516*, 5039−5045.
(40) Crick, S. L.; Yin, F. C.-P. Assessing Micromechanical Properties of Cells with Atomic Force Microscopy: Importance of the Contact Point. *Biomech. Model. Mechanobiol.* **2007**, *6*, 199−210.
(41) Kaufmann, S.; Borisov, O.; Textor, M.; Reimhult, E. Mechanical Properties of Mushroom and Brush Poly(ethylene Glycol)-Phospholipid Membranes. *Soft Matter* **2011**, *7*, 9267−9275.
(42) Garbuzenko, O.; Barenholz, Y.; Priev, A. Effect of Grafted PEG on Liposome Size and on Compressibility and Packing of Lipid Bilayer. *Chem. Phys. Lipids* **2005**, *135*, 117−129.
(43) Hope, M. J.; Bally, M. B.; Webb, G.; Cullis, P. R. Production of Large Unilamellar Vesicles by a Rapid Extrusion Procedure. Characterization of Size Distribution, Trapped Volume and Ability to Maintain a Membrane Potential. *Biochim. Biophys. Acta, Biomembr.* **1985**, *812*, 55−65.
(44) Lee, S.; Bae, S.-S.; Medeiros-Ribeiro, G.; Blackstock, J. J.; Kim, S.; Stewart, D. R.; Ragan, R. Scanning Tunneling Microscopy of Template-Stripped Au Surfaces and Highly Ordered Self-Assembled Monolayers. *Langmuir* **2008**, *24*, 5984−5987.
(45) Hutter, J. L.; Bechhoefer, J. Calibration of Atomic-force Microscope Tips. *Rev. Sci. Instrum.* **1993**, *64*, 1868−1873.
(46) Hegner, M.; Wagner, P.; Semenza, G. Ultralarge Atomically Flat Template-Stripped Au Surfaces for Scanning Probe Microscopy. *Surf. Sci.* **1993**, *291*, 39−46.
(47) Ragan, R.; Ohlberg, D.; Blackstock, J. J.; Kim, S.; Williams, R. S. Atomic Surface Structure of UHV-Prepared Template-Stripped Platinum and Single-Crystal Platinum(111). *J. Phys. Chem. B* **2004**, *108*, 20187−20192.
(48) Li, M.; Chen, M.; Sheepwash, E.; Brosseau, C. L.; Li, H.; Pettinger, B.; Gruler, H.; Lipkowski, J. AFM Studies of Solid-Supported Lipid Bilayers Formed at a Au(111) Electrode Surface Using Vesicle Fusion and a Combination of Langmuir−Blodgett and Langmuir−Schaefer Techniques. *Langmuir* **2008**, *24*, 10313−10323.
(49) Butt, H.-J.; Stark, R. Atomic Force Microscopy in Structured Liquids: Remark on the Interpretation of Jumps in Force Curves. *Colloids Surf., A* **2005**, *252*, 165−168.
(50) Ip, S.; Li, J. K.; Walker, G. C. Phase Segregation of Untethered Zwitterionic Model Lipid Bilayers Observed on Mercaptoundecanoic-Acid-Modified Gold by AFM Imaging and Force Mapping. *Langmuir* **2010**, *26*, 11060−11070.
(51) Kučerka, N.; Nieh, M.-P.; Katsaras, J. Fluid Phase Lipid Areas and Bilayer Thicknesses of Commonly Used Phosphatidylcholines as a Function of Temperature. *Biochim. Biophys. Acta, Biomembr.* **2011**, *1808*, 2761−2771.
(52) Janosi, L.; Gorfe, A. A. Simulating POPC and POPC/POPG Bilayers: Conserved Packing and Altered Surface Reactivity. *J. Chem. Theory Comput.* **2010**, *6*, 3267−3273.
(53) Stan, G.; DelRio, F. W.; MacCuspie, R. I.; Cook, R. F. Nanomechanical Properties of Polyethylene Glycol Brushes on Gold Substrates. *J. Phys. Chem. B* **2012**, *116*, 3138−3147.
(54) Heberle, F. A.; Petruzielo, R. S.; Pan, J.; Drazba, P.; Kučerka, N.; Standaert, R. F.; Feigenson, G. W.; Katsaras, J. Bilayer Thickness Mismatch Controls Domain Size in Model Membranes. *J. Am. Chem. Soc.* **2013**, *135*, 6853−6859.
(55) Bayerl, T. M.; Bloom, M. Physical Properties of Single Phospholipid Bilayers Adsorbed to Micro Glass Beads. A New Vesicular Model System Studied by 2H-Nuclear Magnetic Resonance. *Biophys. J.* **1990**, *58*, 357−362.
(56) Koenig, B. W.; Krueger, S.; Orts, W. J.; Majkrzak, C. F.; Berk, N. F.; Silverton, J. V.; Gawrisch, K. Neutron Reflectivity and Atomic Force Microscopy Studies of a Lipid Bilayer in Water Adsorbed to the Surface of a Silicon Single Crystal. *Langmuir* **1996**, *12*, 1343−1350.
(57) Backmann, N.; Kappeler, N.; Braun, T.; Huber, F.; Lang, H.-P.; Gerber, C.; Lim, R. Y. H. Sensing Surface PEGylation with Microcantilevers. *Beilstein J. Nanotechnol.* **2010**, *1*, 3−13.
(58) Picas, L.; Rico, F.; Scheuring, S. Direct Measurement of the Mechanical Properties of Lipid Phases in Supported Bilayers. *Biophys. J.* **2012**, *102*, L01−03.
(59) Flory, P. J. *Principles of Polymer Chemistry*; Cornell University Press: New York, 1953.
(60) Kenworthy, A. K.; Hristova, K.; Needham, D.; McIntosh, T. J. Range and Magnitude of the Steric Pressure between Bilayers Containing Phospholipids with Covalently Attached Poly(ethylene Glycol). *Biophys. J.* **1995**, *68*, 1921−1936.
(61) De Gennes, P. G. Polymers at an Interface; a Simplified View. *Adv. Colloid Interface Sci.* **1987**, *27*, 189−209.
(62) De Gennes, P. G. Conformations of Polymers Attached to an Interface. *Macromolecules* **1980**, *13*, 1069−1075.
(63) Edwards, K.; Johnsson, M.; Karlsson, G.; Silvander, M. Effect of Polyethyleneglycol-Phospholipids on Aggregate Structure in Preparations of Small Unilamellar Liposomes. *Biophys. J.* **1997**, *73*, 258−266.
(64) Ickenstein, L. M.; Arfvidsson, M. C.; Needham, D.; Mayer, L. D.; Edwards, K. Disc Formation in Cholesterol-Free Liposomes during Phase Transition. *Biochim. Biophys. Acta, Biomembr.* **2003**, *1614*, 135−138.
(65) Hristova, K.; Kenworthy, A.; McIntosh, T. J. Effect of Bilayer Composition on the Phase Behavior of Liposomal Suspensions Containing Poly(ethylene Glycol)-Lipids. *Macromolecules* **1995**, *28*, 7693−7699.
(66) Johnsson, M.; Edwards, K. Liposomes, Disks, and Spherical Micelles: Aggregate Structure in Mixtures of Gel Phase Phosphatidylcholines and Poly(Ethylene Glycol)-Phospholipids. *Biophys. J.* **2003**, *85*, 3839−3847.
(67) Mazer, N. A.; Benedek, G. B.; Carey, M. C. Quasielastic Light-Scattering Studies of Aqueous Biliary Lipid Systems. Mixed Micelle Formation in Bile Salt-Lecithin Solutions. *Biochemistry (Moscow)* **1980**, *19*, 601−615.